ARTICLE TYPE www. rsc.org/xxxxxx | XXXXXXXX

Computational Methodologies and Physical Insights into Electronic Energy Transfer in Photosynthetic Light-Harvesting Complexes

Leonardo A. Pachón[a,b] **and Paul Brumer**[*b]

Received Xth March 2012, Accepted Xth XXXXXXXXX 2012
First published on the web Xth XXXXXXXXXX 2012
DOI: 10.1039/b000000x

We examine computational techniques and methodologies currently in use to explore electronic excitation energy transfer in the context of light-harvesting complexes in photosynthetic antenna systems, and comment on some new insights into the underlying physics. Advantages and pitfalls of these methodologies are discussed, as are some physical insights into the photosynthetic dynamics. By combining results from molecular modelling of the complexes (structural description) with an effective non-equilibrium statistical description (time evolution), we identify some general features, regardless of the particular distribution in the protein scaffold, that are central to light-harvesting dynamics and, that could ultimately be related to the high efficiency of the overall process. Based on these general common features, some possible new directions in the field are discussed.

1 Introduction

The transfer of electronic excitation energy is ubiquitous in nature and its dynamics and manipulation is of special interest in diverse fields of physics, chemistry, biology and engineering. Traditionally, electronic excitation energy transfer (EET) has been studied and described in, e.g., molecular crystals [1], rare gases in the solid phase [2,3] and dye aggregates [4]. More recently focus has turned to EET in biological pigment-protein complexes present in light-harvesting complex of natural photosynthetic antenna systems [5]. The dynamics of the EET process in these systems is often thought of in terms of donors and acceptors of excitation, and it is characterized, mainly, by two time scales: a time scale τ_{da} at which the transfer between donors and acceptors takes place (intermolecular transitions) and a second time scale τ_{vr} at which the intramolecular (vibrational) relaxation occurs [6].

Based on the τ_{da} and τ_{vr} time scales, the field distinguishes between two limiting cases. If the intermolecular transitions are faster than the intramolecular relaxation, $\tau_{vr}/\tau_{da} < 1$, then the exciton is *delocalized* among the donor-acceptor pairs and it travels across the complex *coherently*. If, by contrast, $\tau_{vr}/\tau_{da} > 1$, then the exciton is *localized* and it hops from donors to acceptors, and propagates *incoherently* across the complex. Under *in-vivo* conditions, such as those in photosynthetic light-harvesting complexes [5], EET has been largely considered as incoherent, and its high efficiency ($\lesssim 100\%$) has been discussed in terms of the ultrafast, tens of picoseconds, character of the overall process [7,8]. [An important exception to the incoherent-dynamics assumption is found in, e.g., the Light-Harvesting Complex II (LHCII is present in most of the higher plants) or in the Chlorosomes (found in, e.g., green sulfur bacteria) where, due to the strong coupling between chromophores, the excitations stay delocalized over a certain number of pigments, even at room temperature [8,9].]

Recent experimental results [10–14] have suggested that during the first steps of EET in some light-harvesting complexes, quantum coherences between different monomers of the photosynthetic chromophores may be assisting in the high efficiency of the electronic excitation energy transfer. This provocative suggestion resulted from the observation that these coherences were, apparently, living longer (~ 800 fs at 77 K and ~ 400 fs at 277 K) than could have been predicted (cf. Refs. 15,16 or Sec. 5.2 below). These two issues, and their implications, rapidly became the center of considerable study from diverse fields of chemistry and physics (cf. the review articles in Refs. 17–22).

The initial attempts to explain the dynamics observed in these experiments [10–14] were based on Förster's theory [23,24] (strong exciton-vibrational coupling compared with the dipole-dipole interaction between the donor and acceptor, fast intramolecular relaxation, incoherent transfer) or on the Redfield formalism [25] (weak exciton-vibrational coupling, slow relaxation). These studies revealed that these two approaches were inadequate because, in the dynamics of photosynthetic complexes, there is neither a dominant time scale nor a leading coupling strength [17–22]. This fact motivated the use of approaches and techniques developed in other fields such as quantum optics [26–28], semiclassical molecular dynamics [29–32], solid state physics [16,33,34], etc., and encouraged the development of a variety of new techniques [18,21]. In addition, it motivated the improvement of molecular modelling techniques [17,20,22], in particular in aspects related to the influence of the protein environment, and to the possibility of all-atom

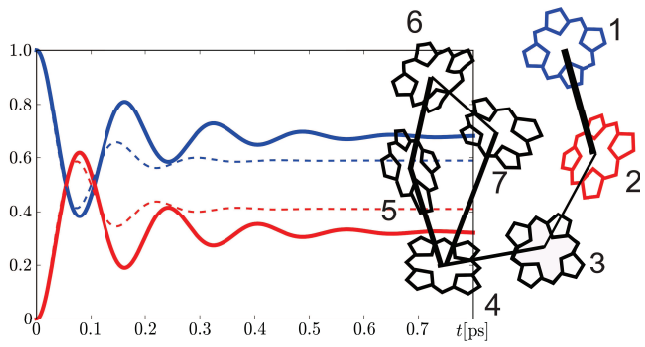

TOC entry: Methodologies used to explore electronic energy transfer in light-harvesting photosynthetic complexes are examined and comments on new insights into the underlying physics are provided.

simulations of the system time evolution[35].

Our goal in this Perspective is to summarize the state-of-the-art in the computational description of EET in photosynthetic complexes as well as to suggest some new possible directions in the field. In doing so, we collect common features that have emerged from the different approaches. We also attempt to collect the relevant physical information that could be used as input for molecular modelling strategies in the potential design of artificial EET systems.

2 Photosynthetic Complexes

Structures of natural light-harvesting antenna complexes are extremely diverse. One can find anything from strcutures that are highly symmetric structures to those where the chromophores seem to be placed randomly in the protein scaffold[8,31,36]. This diversity can be evidenced in, e.g., the interchromophore separation, which is, e.g., ~ 1 nm for organisms with chlorophyll-based networks or more than ~ 2 nm in organisms with bilin-based networks[8,31,36]. Remarkably, in all cases the light harvesting efficiencies in these networks are reported to be close to 100%[8,31,36].

Despite this variability in structure, the chromophore excitation energy/electronic coupling landscape share some similarities that are worth analyzing in order to identify mechanisms that underlie the high efficiency of the photosynthetic transport. We postpone this description until Sec. 5 and, in the following, describe some of the structural features of two of the better studied complexes, the Fenna-Matthews-Olson (FMO) present in green sulfur bacteria and the Phycocyanin-645 (PC645) complex from *Chroomonas* sp., in order to provide a physical picture of these systems. Subsequently, we describe the standard theoretical framework for studying EET[5,6].

[a] *Instituto de Física, Universidad de Antioquia, AA 1226, Medellín, Colombia. Tel: 57 4 219 6439; E-mail: leonardo.pachon@fisica.udea.edu.co*
[b] *Chemical Physics Theory Group, Department of Chemistry and Center for Quantum Information and Quantum Control, University of Toronto, Toronto, Canada M5S 3H6. Fax: 1 416 978 5325; Tel: 1 416 978 7044; E-mail: pbrumer@chem.utoronto.ca*

2.1 Examples: FMO and PC645

The FMO pigment-protein complex from *Chlorobium tepidum*[11,14] is a trimer consisting of identical, weakly interacting monomers[37]. Each weakly interacting FMO monomer contains seven coupled bacteriochlorophyll-*a* (BChl-*a*) chromophores arranged asymmetrically, yielding eight nondegenerate, delocalized molecular excited states (excitons)[11,14]. The coupling values of the seven chromophores, organized as {BChl*a* 1, BChl*a* 2,..., BChl*a* 7}, can be summarized by the following Hamiltonian

$$H_{\rm FMO} = \begin{pmatrix} 240 & -\mathbf{87.7} & 5.5 & -5.9 & 6.7 & -13.7 & -9.9 \\ & 315 & \mathbf{30.8} & 8.2 & 0.7 & 11.8 & 4.3 \\ & & 0 & \mathbf{-53.5} & -2.2 & -9.6 & 6.0 \\ & & & 130 & \mathbf{-70.7} & -17.0 & \mathbf{-63.3} \\ & & & & 285 & \mathbf{81.1} & -1.3 \\ & & & & & 435 & 39.7 \\ & & & & & & 245 \end{pmatrix},$$

where the energy of the third chromophore has be taken as the reference zero. Values are given in units of $\rm cm^{-1}$ in the site representation[37].

Since the electronic coupling between the chromophores BChl*a* 1 and BChl*a* 2 is relatively strong compared to the other coupling strengths[37], see $H_{\rm FMO}$, it is common to focus, for purposes of model studies of EET, on the dynamics of the excitation in a dimer composed by BChl*a* 1 and BChl*a* 2. (This often adopted model is discussed further in Sec. 5).

Although the seven site model has been the standard, an eight bacteriochlorophyll-*a* chromophore was recently discovered[38,39]. In what follows we restrict our discussion to the case of seven chromophores and refer the interested reader to Ref. 33 for a detailed analysis of the influence of the eighth chromophore on the EET dynamics.

The PC645 pigment-protein complex has been studied both experimentally[13] and numerically in great detail[31]. It contains eight bilin molecules covalently bound to the protein scaffold. A dihydrobiliverdin (DBV) dimer is located at the center of the complex and two mesobiliverdin (MBV) molecules located near the protein periphery give rise to the upper half of the complex absorption spectrum. Excitation of this dimer may initiate the light harvesting process[13]. The coupling values of the eight bilin molecules, arranged as {DBVc, DBVd, MBVa, MBVb, PCBc158, PCBd158, PCBc82, PCBs82}, can

be summarized by the following Hamiltonian[13,40]

$$H_{\mathrm{PC645}} = \begin{pmatrix} 17034 & 319.4 & -9.6 & -43.9 & 20.3 & 25.3 & -46.8 & -20.0 \\ & 17116 & 43.9 & 7.7 & 30.5 & 29.0 & 21.5 & 48.0 \\ & & 16050 & 4.3 & -86.7 & -2.9 & -15.8 & 49.3 \\ & & & 16373 & 3.4 & 86.2 & 53.8 & -14.7 \\ & & & & 15808 & 7.8 & 11.0 & 10.0 \\ & & & & & 15889 & 29.0 & -10.7 \\ & & & & & & 15566 & 48.0 \\ & & & & & & & 15647 \end{pmatrix},$$

in units of cm^{-1}. The electronic coupling between the closely spaced DBVc and DBVd molecules is $\sim$320 cm^{-1}. This relatively strong coupling results in the delocalization of the excitation, yielding the dimer electronic excited states labelled DBV+ and DBV−. Excitation energy absorbed by the dimer flows to the MBV molecules which are each 23 Å from the closest DBV, and ultimately to four phycocyanobilins (PCB) that absorb in the lower-energy half of the absorption spectrum[13].

Note that FMO and PC645 play a distinctly different role physically. The former serves to transmit energy from the antenna to the reaction center. That is, under natural conditions light absorption is the function of the outer antenna structure and the probability of photon absorption in the FMO is very low. By contrast, PC645 does, naturally, play an active role in absorbing incident radiation.

2.2 Hamiltonian

Theoretical modelling of the exciton energy transfer process comprises intramolecular and intermolecular contributions (cf. Chap 9 in Ref. 6, or Ref. 5) and involves a number of assumptions, noted below, regarding the presumed physics. For the particular case of a pigment-protein complex composed of N pigments, the corresponding Hamiltonian, H_{ppc},

$$H_{\mathrm{ppc}} = \sum_{m=1}^{N} H_m(\mathbf{r}_m, \mathbf{R}_m) + \sum_{m,n\geq m} V_{mn}(\mathbf{r}_{mn}, \mathbf{R}_{mn}), \qquad (1)$$

where H_m describes intra-pigment contributions and V_{mn} contains all the inter-pigment Coulomb interactions. The Hamiltonian of the m-th pigment is characterized by the electronic coordinates $\mathbf{r}_m$ and the nuclear coordinates $\mathbf{R}_m$ and can be decomposed as $H_m = T_m^{(\mathrm{nuc})} + H_m^{(\mathrm{el})}$, where $T_m^{(\mathrm{nuc})}$ denotes the nuclear kinetic energy contribution. Since we are not considering electron transfer among different pigments, we can expand the pigment-protein complex Hamiltonian in terms of the adiabatic electronic states $\{\varphi_{ma}(\mathbf{r}_m;\mathbf{R}_m)\}$ defined by $H_m^{(\mathrm{el})}(\mathbf{R}_m)\varphi_{ma}(\mathbf{r}_m;\mathbf{R}_m) = U_{ma}\varphi_{ma}(\mathbf{r}_m;\mathbf{R}_m)$, where a refers to the a-th state of pigment m and $U_{ma}(\mathbf{R}_m)$ denotes the corresponding single-molecule potential energy surface (PEF).

The inter-pigment interactions in Eq. (1) depend on the distance $\mathbf{r}_{mn}$ between the electrons in the pigment m and those in the pigment n, as well as on distance $\mathbf{R}_{mn}$ between the electron in pigment m and the nuclei of pigment n. These interactions comprise the electron-electron interaction $V_{mn}^{\mathrm{el-el}}$ and electron-nuclei interactions $V_{mn}^{\mathrm{el-nuc}}$. As discussed in Sec. 2.2.2.1, the coupling to the nuclear degrees of freedom can be identified as the first source of electronic decoherence.

The transfer of electronic excitation energy is often accompanied by the transfer of electrons[6,41]. However, it is generally assumed that the pigments are sufficiently far apart so that the intermolecular wave functions do not overlap $\left(\langle\varphi_{ma}|\varphi_{nb}\rangle = \delta_{ma,nb}\right)$. Under these circumstances, the intermolecular interchange can be neglected. As such, we are neglecting the bridge-mediated electron transfer (cf. Ref. 41 or Chap. 7 in Ref. 6) that could induce long-range super exchange of electrons[41] . Nonetheless, one has to be aware that strong coupling to the solvent degrees of freedom can induce overlapping of the intermolecular wave functions.

We shall also restrict ourselves to the situation when the electronic ground state $S_0 = g$ and the first excited singlet state $S_1 = e$ of the different pigments suffice for describing the dynamics of EET. This is the well known two-level model[6]. Additionally, any non-adiabatic transitions between S_0 and S_1 during EET are neglected.

After projecting the Hamiltonian in Eq. (1) onto the set of states defined by the Hartree product ansatz $\{\prod_{m=1}^{N}\varphi_{ma_m}(\mathbf{r}_m;\mathbf{R}_m)\}$, we get[6]

$$\begin{aligned} H_{\mathrm{ppc}} = &\sum_m \sum_{a=g,e} H_{ma}|\,\varphi_{ma}\,\rangle\langle\,\varphi_{ma}\,| \\ &+ \sum_{m,n} J_{mn}|\,\varphi_{me}\varphi_{ng}\,\rangle\langle\,\varphi_{ne}\varphi_{mg}\,|, \end{aligned} \qquad (2)$$

where the matrix elements $H_{ma} = \langle\,\varphi_{ma}\,|H_m|\,\varphi_{ma}\,\rangle$ and $J_{mn} = \langle\,\varphi_{me}\varphi_{ng}\,|V_{mn}|\,\varphi_{ne}\varphi_{mg}\,\rangle$.

From the pigment-protein complex Hamiltonian in Eq. (2), it is clear that the electronic energies H_{ma} as well as the excitonic couplings J_{mn} depend upon the nuclear coordinates. As discussed below, they also depend upon the external environment (solvent), so that, in general, their values are constrained by the underlying interactions. Methodologies and strategies for obtaining these parameters are discussed in Sec. 4.

2.2.1 The site representation—The transfer of electronic excitation energy can be described in terms of the number of excitations present in the complex. If no excitations are present, then the complex is in its ground state, $|\,0\,\rangle = \prod_m|\,\varphi_{mg}\,\rangle$. In the case when a single excitation resides at pigment m, it is denoted $|\,m\,\rangle = |\,\varphi_{me}\,\rangle\prod_{n\neq m}|\,\varphi_{ng}\,\rangle$. This ordering of states suggests the following decomposition of the Hamil-

tonian in Eq. (2),

$$\begin{aligned} H_{\rm ppc} &= H^{(0)}_{\rm ppc} + H^{(1)}_{\rm ppc} + \dots \\ &= \sum_m H_{mg} |0\rangle\langle 0| \\ &+ \sum_m \left(H_{me} + \sum_{n\neq m} H_{ng} \right) |m\rangle\langle m| + \sum_{m,n} J_{mn} |m\rangle\langle n| \\ &+ \dots, \end{aligned} \tag{3}$$

where the second line in Eq. (3) denotes the Hamiltonian of the zero-exciton manifold and the third line denotes the single-exciton manifold Hamiltonian. In Eq. (3), the intermolecular electrostatic coupling has been neglected[6]. In general, the description of the dynamics in terms of the *n*-exciton manifolds is known as the site representation.

2.2.2 Exciton-vibrational interactions—As already discussed, in addition to the solvent, the vibrational degrees of freedom comprise contributions from the single-pigment vibrations and from inter-pigment vibrations[6]. The role of these vibrational degrees of freedom (DOF) is twofold: apart from modulating the electronic energies and the excitonic couplings in Eq. (2) or in Eq. (3), they are a source of electronic decoherence in cases where the vibrations are not measured. As explained below, in such a case the electronic degrees of freedom constitute the system, whereas the vibrations serve as the environment. Note that Sec. 2.2.2.1 contains a fulldiscussion of how the nuclear degrees of freedom can induce electronic decoherence.

Note that, following Refs. 5 and 6, we also effectively include the effects of the vibrations as well as the influence of the solvent (environment or reservoir) around the pigments. In Sec. 2.4, we discuss the characterization of this effective model of the vibrations and the environment from a statistical point of view.

2.2.2.1 Electronic decoherence by vibrational DOF. As an example, consider the excitation from an initial product state comprising the ground electronic state $|g\rangle$ and the ground vibrational state $|v_g\rangle$ to an excited electronic state $|e\rangle$ in a single pigment. For a sufficiently fast laser pulse, the state of the pigment will be described by the density matrix

$$\begin{aligned} \rho_{tot} = A^2 \Big(&|g\rangle|v_g\rangle\langle v_g|\langle g| + |c|^2 |e\rangle|v_g(t)\rangle\langle v_g(t)|\langle e| \\ &+ c^* |g\rangle|v_g\rangle\langle v_g(t)|\langle e| e^{i\delta t\hbar} + c|e\rangle|v_g(t)\rangle\langle v_g|\langle g| e^{-i\delta t\hbar} \Big), \end{aligned} \tag{4}$$

where A is a normalization constant, c is proportional to the dipolar element $d_{e,g}$ and δ is the difference in energy between the minima in the nuclear potential on the ground and excited electronic states.

Since our interest is in the electronic dynamics then, assuming the Condon approximation is valid, we trace over the vibrational states and get the density matrix for the electronic degrees of freedom:

$$\begin{aligned} \rho = A^2 \Big(&|g\rangle\langle g| + |c|^2 |e\rangle\langle e| + c^* |g\rangle \langle v_g(t)|v_g\rangle \langle e| e^{i\delta t\hbar} \\ &+ c|e\rangle\langle g| \langle v_g|v_g(t)\rangle e^{-i\delta t\hbar} \Big). \end{aligned} \tag{5}$$

The electronic coherence, manifested in the off-diagonal matrix elements $|g\rangle\langle e|$ and $|e\rangle\langle g|$, is modulated by the overlap $\langle v_g(t)|v_g\rangle$. As the vibrational wave packet $|v_g(t)\rangle$ evolves on the upper electronic surface, particularly when the wavepacket comprises many states, the overlap $\langle v_g(t)|v_g\rangle$ can decrease and so will the off-diagonal terms; the result is electronic decoherence (cf. Refs. 42 and 43 or Chap. 6 in Ref. 44).

This process, electronic decoherence by the vibrational states, has been widely studied using quantum/classical methodologies[42,43,45–47] and it is expected to occur on ultrashort time scales. For example, results on betaine dye molecules[45] and on femtosecond dynamics and laser control of charge transport in trans-polyacetylene[46,47] suggest that these time scales are very short, ∼2.5 fs and ∼3.7 fs, respectively. We return to this subject in Sec. 5, because it is the comparison of these time scales to those observed experimentally, which are far longer, that has motivated a great deal of research.

In our description we have assumed that the each pigment is affected only by its local vibrations, which are assumed to be uncorrelated. However, which degrees of freedom are to be regarded as the bath and what is the nature of the vibrations is crucial to the decoherence issue[48]. For example, it has been shown that if the correlations between local vibrations are taken into account, they could suppress the cross-over to incoherent dynamics at high temperatures[49] or affect the trapping time in rings of chromophores[50]. This subject is widely discussed in Ref. 51 and more recently in Ref. 52, references to which the reader is referred.

2.2.2.2 Inclusion of the intra/inter vibrational DOFs and the solvent. As a first approximation, one could assume that the nuclear motion as well as the low-frequency solvent coordinates can be treated in the harmonic approximation and attempt to simulate its effects via a set of dimensionless vibrational normal mode coordinates $\{q_\alpha\}$ of frequency ω_α. In this case, the Hamiltonian for the ground state contribution of the pigment-protien-complex in Eq. (3) now reads

$$H^{(0)}_{\rm ppc} = \mathscr{H}_0 |0\rangle\langle 0| \tag{6}$$

$$\mathscr{H}_0 = E_0 + \sum_m H_{mg} + \sum_\alpha \hbar\omega_\alpha b^\dagger_\alpha b_\alpha \tag{7}$$

where E_0 denotes the ground state energy, including vibrational zero-point energies, of the normal-mode vibrations[6]. $b_\alpha^\dagger$ and b_α are the annihilation and creation operators, respectively, expressed in terms of the normal mode coordinates $Q_\alpha = (b_\alpha^\dagger + b_\alpha)$ with $q_\alpha = \sqrt{\hbar/2\omega_\alpha}Q_\alpha$.

Assuming that the ground and the singly excited electronic states can be described by the same normal coordinates, the single excitonic Hamiltonian reads[6]

$$H_{\rm ppc}^{(1)} = \sum_{m,n} \mathscr{H}_{mn} |m\rangle\langle n| \tag{8}$$

$$\begin{aligned}\mathscr{H}_{mn} &= \delta_{mn}H_{me} + (1-\delta_{mn})\left[J_{mn}^{(0)} + \sum_\alpha \hbar\omega_\alpha \tilde{g}_{mn}(\alpha)Q_\alpha\right] \\ &+ \delta_{mn}\left[\sum_{k\neq m} H_{kg} + \sum_\alpha \hbar\omega_\alpha\left(b_\alpha^\dagger b_\alpha + \frac{1}{2} + g_m(\alpha)Q_\alpha\right)\right].\end{aligned} \tag{9}$$

The exciton-vibrational coupling matrix $g_{mn}(\alpha) = \delta_{m,n}g_m(\alpha) + (1-\delta_{m,n})\tilde{g}_{mn}(\alpha)$ in Eq. (9) is given by the dimensionless coupling constants $g_m(\alpha)$, determined from the linearization of the potential energy surfaces along the normal modes, and by the coupling constants $\tilde{g}_{mn}(\alpha)$, which account for the influence of the vibrational motions in the electronic couplings J_{mn}^0. In the Frank-Condon approximation, vibrational motion does not induce electronic transitions; that is, $g_{mn}(\alpha) = \delta_{m,n}g_m(\alpha)$.

2.3 Summary of the assumptions and approximations

It is useful to summarize the approximation made in deriving Eqs. (7) and (9), which is essentially the Frenkel-exciton model. Assumption one is the absence of inter-pigment electron transfer, which is guaranteed if there is no intermolecular wave function overlap, e.g., if the pigments are sufficiently far apart. Second, the EET dynamics is assumed to be fully characterized by the electronic ground state $S_0 = g$ and the first excited singlet state $S_1 = e$ of each pigment, yielding " the two-level model".

In the next step one couples the electronic manifolds to the vibrational nuclear modes and to the solvent coordinates, which induce decoherence and dissipation. For simplicity, we have assumed no inter-pigment electronic-nuclear interactions, so that nuclear vibrations pertain to each pigment. Additionally, we assume that the collective nuclear-solvent vibrations can be described by a global manifold in its harmonic approximation. Since the dipole-interaction matrix elements will depend, in general, upon this collective coordinate, we further adopt the Frank-Condon approximation and neglect any possible non-adiabatic transitions induced by the solvent. This set of approximation results in Eqs. (7) and (9).

2.4 Dissipation and Decoherence

Since the number of nuclear and solvent degrees of freedom (DOF) in Eq. (8) is extremely large, one could invoke a statistical treatment of those DOF. From a statistical viewpoint the combined effects of the vibrational states and the solvent in each pigment in Eq. (8) can be described in terms of a local fluctuating random force $\zeta_m(t)$ describing the fluctuations of the position-normal-mode coordinate. Each of these fluctuating forces can be characterized in terms of its two-time correlation function $\langle\zeta_m(t)\zeta_m(0)\rangle_{mg}$, where $\langle\rangle_{mg}$ denotes statistical average over the equilibrium density operator, $\rho_{mg}^{\rm eq} = \exp(-H_{mg}\beta)/{\rm tr}[\exp(-H_{mg}\beta)]$, of the normal modes in Eq. (9). For the particular case described in Eq. (9), the correlation function is be defined by[53–56]

$$\begin{aligned}\langle\zeta_m(t)\zeta_m(0)\rangle_{mg} &= \hbar\int_0^\infty \frac{{\rm d}\omega}{\pi} J_m(\omega) \\ &\left[\coth\left(\frac{\hbar\beta\omega}{2}\right)\cos(\omega t) - {\rm i}\sin(\omega t)\right].\end{aligned} \tag{10}$$

where $\beta = 1/k_{\rm B}T$, T is the temperature of the combined environment and $J_m(\omega)$ is termed the spectral density (see Sec. 2.4.1 below). The fact that $\langle\zeta_m(t)\zeta_m(0)\rangle_{mg}$ is complex is a consequence of the anticommutativity of the normal mode coordinates p_α and q_α[55]. In the classical limit, $\hbar \to 0$, the correlation function is real and becomes

$$\langle\zeta_m(t)\zeta_m(0)\rangle_{mg} \to \frac{2}{\pi\beta}\int_0^\infty \frac{{\rm d}\omega}{\omega} J_m(\omega)\cos(\omega t) = \frac{1}{\beta}\Gamma_m(t), \tag{11}$$

where $\Gamma_m(t)$ is the relaxation function. $\Gamma_m(t)$ is the directly observable quantity in time-dependent fluorescence Stokes shift experiments[15,18] and is defined in terms of the reorganization energy λ_m as $\Gamma_m(0) = 2\hbar\lambda_m$[57]. From $\Gamma_m(t)$, the relaxation time τ_m of the environment can be determined as $\tau_m = \frac{1}{\Gamma_m(0)}\int_0^\infty {\rm d}t\Gamma_m(t)$.

2.4.1 The spectral density.— The spectral density contains the relevant information about the nature of the environment and is usually chosen to fit some measurable quantity, e.g., the optical spectrum, of the system. As discussed in Sec. 4, spectral densities may also be obtained from computational methods (cf. Refs. 37,58). Here again the idea is that the dynamical features, usually classically described, be in agreement with the optical measurable quantities. The complexity of obtaining reliable spectral densities is indicated by the studies in Ref. 58, where a host of highly structured spectral densities are shown for FMO. In the following, we restrict attention to the spectral densities already used for studying the dynamics of EET.

For the particular case of the FMO complex, e.g., Adolphs and Renger[37] derived a spectral density which allows calculations that show agreement between the experimental optical

spectrum and calculations based on pigment transition energies. This spectral density is given by

$$J_{\rm FMO}(\omega) = \omega^2 S_0 g_0(\omega) + \omega^2 S_{\rm H}\delta(\omega-\omega_{\rm H}), \qquad (12)$$

with $S_0 = 0.5$, $S_{\rm H} = 0.22$, $\omega_{\rm H} = 180$ cm^{-1}. The spectral density $J_{\rm FMO}(\omega)$ comprises two parts, one related to protein vibrations and characterized by $g_0(\omega) = 6.105\times10^{-5}\times(\omega^3/{\omega_1}^4)\mathrm{e}^{-\sqrt{\omega/\omega_1}} + 3.8156\times10^{-5}\times(\omega^3/{\omega_2}^4)\mathrm{e}^{-\sqrt{\omega/\omega_2}}$, $\omega_1 = 0.575$ cm^{-1}and $\omega_2 = 2$ cm^{-1}, and the other associated with a vibrational mode characterized by the Dirac delta function in Eq. (12). This spectral function was recently used in Ref. 34 to study the dynamics of the FMO complex and the results are discussed in Sec. 3.2.2. A comparison of this spectral density function and that computed recently[58] is provided in Sec. 4 below.

Another type of spectral density widely used in the context of EET, as well as in non-linear spectroscopy, is the Ohmic model with Lorentz-Drude regularization[15,18,21,56,57,59]

$$J_m(\omega) = 2\hbar\lambda_m\tau_m\omega/\left(1+\omega^2\tau_m^2\right). \qquad (13)$$

For this case, the relaxation function reads $\Gamma_m(s) = 2\hbar\lambda_m\exp(-s/\tau_m)$. A variant to the Lorentz-Drude regularization model is the Ohmic spectral density with exponential decay[16,56,60]

$$J_m(\omega) = 2K\omega\exp(-\omega/\omega_{\rm c}), \qquad (14)$$

where the dimensionless parameter K describes the damping strength and $\omega_{\rm c}$ is the cut-off frequency. For this variant, the reorganization energy is given by $\lambda_m = 2K_m\hbar\omega_{{\rm c},m}$ and the relaxation time by $\tau_m = \pi/(2\omega_{{\rm c},m})$. The Ohmic spectral density with exponential decay is a member of a more general family of spectral densities parametrized by s as $J(\omega)\sim\omega^s\mathrm{e}^{-\omega/\omega_{\rm c}}$. Here, $s=1$ is the Ohmic spectral density while $s<1$ ($s>1$) is termed the sub-Ohmic (super Ohmic) spectral densities[56]. Although the Ohmic spectral density is a useful choice for, e.g., electron transfer dynamics or biomolecular complexes[6,61], it has the drawback that it does not contain any high-frequency modes of the environment.[34,58,62].

Another relevant spectral density is the one characterizing the effect of blackbody radiation (e.g., natural sunlight or moonlight)[63–68]. From an open-quantum-system perspective, the influence of the blackbody radiation is condensed in the spectral density[69–72]

$$J_{\rm BB}(\omega) = M\tau_{\rm BB}\,\omega^3\Omega_{\rm BB}^2/\left(\Omega_{\rm BB}^2+\omega^2\right), \qquad (15)$$

where $M_{\rm e} = m + M_{\rm e}\tau_{\rm BB}\Omega_{\rm BB}$ is the renormalized mass of the electron (whose bare mass is m), $\tau_{\rm BB} = 2e^2/3M_{\rm e}c^3\sim 6.24\times10^{-24}$s and $\Omega_{\rm BB}$ is a frequency cutoff[69–71]. For this spectral density, the decay function in Eq. (11) is $\Gamma_{\rm BB}(s) = \tau_{\rm BB}\Omega_{\rm BB}^2\left[2\delta(s)-\Omega_{\rm BB}\exp(-\Omega_{\rm BB}|s|)\right]$. In the limit $\Omega_{\rm BB}\to\infty$, one gets the surprising result $\Gamma_{\rm BB}(s)=0$. This corresponds to taking the point-electron limit. An interesting feature of Eq. (15) is that it is capable of introducing fluctuations without dissipation, with no violation of the fluctuation-dissipation theorem[73]. As such, it provides a sound statistical mechanical formulation for the pure-dephasing approaches (cf. Refs. 27,28). We have explored the excitation of open quantum systems by blackbody radiation in Ref. 68 and some associated comments are given in Sec. 5.

3 Spectral-Density Based Approaches

The fact that in photosynthetic light-harvesting complexes there is neither a dominant time scale nor a leading coupling strength[17–22] means that modelling the excitation energy transfer demands the use of robust techniques beyond conventional theoretical approaches such as Förster's theory[23,24], or Redfield[25] or Lindblad equations[74,75]. Due to the various approximations employed in these methodologies, such as the use of perturbation theory in the system-environment coupling strength[18,76,77], the incoherent transfer approximation[18,77,78], the assumption og Markovian dynamics[76,77], or the secular approximation[18,77], these approaches can provide inaccurate descriptions of light-harvesting dynamics. They are therefore of limited applicability when treating realistically parametrized models of light harvesting complexes[29].

Before discussing recent approaches, it is worth discussing the most basic theory for EET: the Förster theory[23,24]. As already noted above, the theory developed by Förster applies to the case of incoherent EET, i.e., to the case when the intermolecular transfer times are slower than the intramolecular relaxation. This approach is based on the Fermi golden rule and on a second order approximation to the excitonic coupling between pigments. This implies that Förster's theory describes EET for weak exciton coupling. Förster's theory characterizes EET in terms of excitation rates $k_{m\to n}$ from pigment m to n. These rates are given in term of the spectral overlap between the donor emission and acceptor absorption spectra and determined by[6,23,24]

$$k_{m\to n} = |J_{mn}|^2\int_{-\infty}^{\infty}\frac{\mathrm{d}\omega}{2\pi}\Re[A_n(\omega)]\Re[F_m(\omega)], \qquad (16)$$

where $F_m(\omega) = \int_0^\infty \mathrm{d}t\,\mathrm{e}^{\mathrm{i}\omega t}\mathrm{e}^{-\mathrm{i}(\omega_m-2\lambda_m)t-g_m^*(t)}$ denotes the emission spectrum of the pigment m and $A_n(\omega) = \int_0^\infty \mathrm{d}t\,\mathrm{e}^{\mathrm{i}\omega t}\mathrm{e}^{-\mathrm{i}\omega_n t-g_n(t)}$ denotes the absorption spectrum of the pigment n. Here, $g_m(t)$ is the line-broadening function[18,57,79]. Within the second-order cumulant expansikon (not required in the original Forster theory), $g_m(t)$ is given by:

$$g_m(t) = \frac{1}{\hbar^2}\int_0^t \mathrm{d}s_1\int_0^{s_1}\mathrm{d}s_2\langle\zeta_m(s_2)\zeta_m(0)\rangle_{mg}\,. \qquad (17)$$

This expression clearly shows that the dynamics, as well as the transport properties, depend on the statistics of the bath as well as on the non-local (in time) character of the correlation function.

We note that at present, in the related open-quantum-system community, there is a great interest in quantifying the non-Markovian (non-local in time) character of dynamics of given systems. In doing so, some measures for the degree of non-Markovian behavior have been given in Refs. 80 and 81. An interesting connection betweemn our discussion above and that subject can be made as follows. The intermediate integral over s_2 in Eq. (17) accounts for the non-Markovian character of the dynamics. This characteristic feature could be useful in order to *experimentally* quantify the non-Markovian character of a particular system based on its line-broadening function. Work along this direction is currently in progress [82].

Below, we divide the discussion into two main parts. In Sec. 3.1, we discuss some of the main methodologies based on master equation descriptions while in Sec. 3.2 we discussed those based on the propagating function.

3.1 Master-equations

Master equation approaches provide equations for the propagation of the density matrix for the system dynamics (here the electrons), obtained by tracing over the environmental degrees of freedom. Popular master-equations based approaches for studying EET are the second-order perturbative time-convolution (TC2) and the second-order perturbative-time convolutionless (TCL2) quantum master equations (see Chap. 9 in Ref. 83 for a formal basis of these techniques) and the hierarchical second-order cumulant expansion approach [18,77,84]. These approaches are based on the projection operator technique [85,86]. The interested reader may find useful the discussions in Refs. 83,85–88.

A comprehensive and detailed discussion regarding the applicability of these three methodologies using typical values present in photosynthetic complexes, $J_{mn} \sim 100$ cm^{-1}, $\lambda_{mn} \sim 100$ cm^{-1}, $E_m \sim 100$ cm^{-1} and $\tau_m \sim 50$ cm^{-1} at 77 and 300 K for the dimer composed of $|\varphi_{1e}\rangle|\varphi_{2g}\rangle$ and $|\varphi_{1g}\rangle|\varphi_{2e}\rangle$, was presented in Ref. 18. For completeness, we briefly discuss only the main features of these approaches.

– TC2 is calculated in second-order perturbative approximation with respect to the coupling of the system to the environment in the interaction picture [83,85,86,88]. Neglecting initial correlation between the pigments and the solvent/vibrational DOFs, in this approach, the time evolution of the system density matrix is calculated as (cf. Chap. 9 in Ref. 83)

$$\frac{\partial}{\partial t}\rho(t) = \sum_{m=1}^{N}\int_{t_0}^{t} \mathrm{d}s \mathscr{K}_m(t,s)\rho(t), \qquad (18)$$

where $\mathscr{K}_m(t,s)$ is the convolution or memory kernel [83]. The equation (18) is a simplified version of the Nakajima-Zwanzig equation [85,86]. Although, the non-local character of this integro-differential equation accounts for the non-Markovian character of the dynamics, it also makes Eq. (18) cumbersome to implement. Thus, further approximations/assumptions are needed.

Using a classical version of the fluctuation-dissipation theorem [equivalent to taking the high temperature limit for the real part of the correlation function of the noise in Eq. (10)], it was shown in Ref. 18 that the transition rates predicted by the TC2 equation deviate strongly from that given by the Markovian Redfield equation as well as from those predicted Förster theory [18]. The authors in Ref. 18 conclude that the TC2 equation is applicable only for the nearly Markovian regime, in spite of its non-Markovian nature.

In Ref. 89 it was shown that the Markovian approximation to the TC2 gives reliable results only for small reorganization energies ($\lambda_m < 10$ cm^{-1} for typical values of EET in photosynthetic complexes ~ 100 cm^{-1}). This is far from the domain relevant to light harvesting.

– TCL2 is based on the TC2 plus the application of the time-convolutionless projector operator technique of Shibata *et al.* [90], which allows for a time local description of the master equation in Eq. (18). TCL2 is accurate for describing coherence between electronic ground and excited states in a monomer, regardless of the magnitude of the electron-phonon coupling [18]. However, as pointed out in Ref. 18, TCL2 fails to describe the transfer rate in a region of large reorganization energy, $\lambda_m > 20$ cm^{-1}. For small reorganization energies, the rate predicted by the TCL2 equation is virtually the same as that for the Markovian Redfield equation [18].

– Second Order Cumulant and Hierarchy Expansion. This strategy allows for the inclusion of site-dependent reorganization energies as well as an appropriate description of the Gaussian fluctuations of the bath [18,77,84]. On the basis of the high temperature approximation, this approach has been used as a benchmark and as a reference in the field because it is able to extrapolate between the Redfield and Förster theories. However, it is restricted to bilinear system-bath coupling, and places very large demands on memory [32]. Further, the numerical effort grows rapidly with increasing system size, and with spectral densities that deviate from the Lorentz-Drude form [91]. Notwithstanding, this approach has the advantage that can be implemented to be numerically exact and is currently used by many research groups (cf. Refs. 18,92).

Note that 77 K corresponds to ~ 50 cm^{-1}, and 300 K to ~ 200 cm^{-1}. These are the typical temperatures at which the 2DPE experiments have been done. One can immediately see that the high temperature condition $\hbar E_m/k_{\mathrm{B}}T \ll 1$ adopted above in some approaches above is barely fulfilled for light-harvesting photosynthetic complexes ($\hbar E_m/k_{\mathrm{B}}T \sim 2$ at 77 K and $\hbar E_m/k_{\mathrm{B}}T \sim 0.5$ at 300 K). In order to be applicable to

other physical scenarios, where the deviations from the high temperature are larger, it would be of interest to efficiently extend these methodologies to the low temperature regime.

3.2 Propagating-function methods

The second main category of approaches relies directly on the propagating function of the system and bath density matrix. We discuss below three of the most commonly used: linearized-density-matrix-dynamics approaches, the quasi-adiabatic propagator path integral (QUAPI) and the non-interacting-blip approximation (NIBA).

3.2.1 Linearized-density-matrix-dynamics—Linearized approaches[29–32,93–98] for quantum evolution were developed in order to deal with non-adiabatic chemical processes such as proton and electron transfer in solution, excited-state molecular fragmentation or molecular relaxation after electronic photo excitation[96,97]. In general, these approaches assume a quantum system represented by a number of discrete basis states $|n\rangle$ coupled to an, in principle highly dimensional, environment described by continuous coordinates $(\hat{Q},\hat{P})$ (cf. Ref. 29). The Hamiltonian for such a system, in the diabatic representation, is given by

$$\hat{H} = \hat{P}^2/2M + \sum_{\lambda} h_{\lambda\lambda}(\hat{Q})|\lambda\rangle\langle\lambda| + \sum_{\lambda<\lambda'} h_{\lambda\lambda'}(\hat{Q})\left(|\lambda\rangle\langle\lambda'| + |\lambda'\rangle\langle\lambda|\right). \quad (19)$$

The first term represents the nuclear kinetic term while the remaining terms comprise the electronic Hamiltonian. Note that the Hamiltonian in Eq. (19) is analogous to that in Eq. (8).

An important ingredient in these approaches[29–32,93–98] is to map the discrete quantum states onto continuous coordinates. The strategy is based on the mapping formalism[93–95]. The idea is to replace the evolution of the electronic subsystem with the evolution of a system of fictitious harmonic oscillators[97]. This is achieved in two steps: (i) Map the electronic Hilbert space spanned by the n diabatic states into one coinciding with a subspace of n harmonic oscillators of unit mass and at most one quantum of excitation in a single specific oscillator[97], i.e., $|\alpha\rangle \rightarrow |m_\alpha\rangle = |0_1,\ldots 1_\alpha \ldots, 0_n\rangle$, and (ii) replace the projection operator by harmonic oscillator creation and annihilation harmonic operators, $|\lambda\rangle\langle\lambda'| \rightarrow \hat{a}^\dagger_\lambda \hat{a}_{\lambda'}$, and express these in terms of their oscillator coordinates and momenta $(\hat{q}_\alpha,\hat{p}_\alpha)$, $\hat{a}_{\lambda'} = (\hat{q}_{\lambda'} + \mathrm{i}\hat{p}_{\lambda'})/\sqrt{2\hbar}$. Once the mapping is performed, the original Hamiltonian in Eq. (19) becomes

$$\hat{H}_{\mathrm{m}} = \hat{P}^2/2M + \frac{1}{2}\sum_{\lambda} h_{\lambda\lambda}(\hat{Q})\left(\hat{q}^2_\lambda + \hat{p}^2_\lambda - \hbar\right) + \frac{1}{2}\sum_{\lambda,\lambda'} h_{\lambda\lambda'}(\hat{Q})\left(\hat{q}_\lambda\hat{q}_{\lambda'} + \hat{p}_\lambda\hat{p}_{\lambda'}\right). \quad (20)$$

The density matrix is evolved according to $\rho(t) = \mathrm{e}^{-\mathrm{i}\hat{H}_{\mathrm{m}}t/\hbar}\rho(0)\mathrm{e}^{\mathrm{i}\hat{H}_{\mathrm{m}}t/\hbar}$. Thus, the resulting Hamiltonian is expressed completely in terms of operators with continuous spectra. Despite this fact, it is able to mimic the effects of transition among discrete electronic states[29,98].

The second main ingredient in the different linearized approaches is the linearization itself. To do this, the unitary time-evolution operator $\mathrm{e}^{-\mathrm{i}\hat{H}_{\mathrm{m}}t/\hbar}$ is represented in terms of discrete phase space path integrals in the environmental variables and double sums over the quantum states[29,98]. From the semiclassical perspective, the evolution of the density matrix is governed by forward and backward trajectories associated with the unitary time-evolution operator and its adjoint operator, respectively. The way in which the action is linearized in the different approaches is what distinguishes between them; the particularities of each are discussed below.

In the linearized approximation to the semiclassical initial value representation (LSC-IVR) of the unitary time-evolution operator (cf. Ref. 30), the action in the path integral expression is expanded to linear order in the distance between the forward and the backward trajectory of the environmental and electronic degrees of freedom. Thus, the the effect of the bath (nuclear degrees of freedom) on the dynamics of the system and the dynamics of the systems itself are approximated. This approach was used in the past[93–95] and more recently used for the particular case of the FMO complex by Tao and Miller[30]. Despite the level of approximation, their results for the dimer case are in agreement with those of Ishizaki and Fleming[18,21]. However, when the full complex is considered, the results at this level of approximation are not reliable[31,32].

In the linearized approach to nonadiabatic dynamics using the mapping formalism (LANDmap)[29,31,97], the linearization is performed only in the environmental degrees of freedom. LANDmap has been used for studying the dynamics of the FMO complex in Ref. 29 as well as the dynamics of the PC645 complex in Ref. 31. In particular, results from Ref. 29 show that when the bath relaxation is slow (e.g., $\tau_{\mathrm{c}} \sim 500$ fs) results obtained with LANDmap are reliable for times around 1 ps at high temperature (~ 300 K) and for a wide range of reorganization energies [$\lambda \sim 0-5\Delta$, being Δ the strength of the electric coupling ($\Delta = 100$ cm^{-1} in Ref. 29)]. For fast relaxation (e.g. $\tau_{\mathrm{c}} \sim 100$ fs) and low temperature (~ 77 K) LANDmap approach provides a reasonable representation of the population oscillations only for short times (~ 100 fs) and for small reorganization energies ($\lambda < \Delta/5$); for this set of parameters, LANDmap is expected to fail to reproduce thermalization[29,31].

LANDmap can be used to generate a short time propagator, which can be iterated to generate more reliable results in the long time regime and valid for a wider spectrum of parameters; this scheme is known as the iterative linearized density

matrix (ILDM) approach[29,98]. Although ILDM is more accurate than LANDmap, its convergence after many iterations can be problematic[32] and it is more demanding in computational terms.

The use of the mapping formalism brings its own drawbacks, in particular when implemented and accompanied by semiclassical approximations (cf. Ref. 32 for details). To circumvent these problems, Huo and Coker have developed an improved version of ILDM: the partial linearized density matrix (PLDM)[32]. It is based on a coherent state representation of the electronic part and a linearization of the nuclear (environmental) degrees of freedom. This approach was tested for nonadiabatic multi states scattering problems and it compared very well with standard results[18]. An important feature of this new approach is the good performance at long times and the correct equilibration with the thermal bath. However, being based on a coherent state representation, PLDM suffers from an excess of free parameters[99–101]. However, the additional parameters can be used to improve the convergence of the average results.

The advantage of the linearized approaches is that they can be applied, in principle, to any molecular model with arbitrary system bath interactions. In particular, PLDM offers a favorable balance between accuracy and computation efficiency[32].

3.2.2 QUAPI-based methods—The quasi-adiabatic propagator path integral (QUAPI)[102–104] has been extensively used by Nalbach and Thorwart in the context of EET[34,105,106]. As in previous approaches, QUAPI assumes that the density matrix of the donor-acceptor system plus the environment can be characterized by a product state at $t = 0$, i.e. $\rho(0) = \rho_{\rm da} \otimes \rho_{\rm env}$. The time evolution of $\rho_{\rm da}(t)$ is obtained after tracing out the environmental (or bath) degrees of freedom, i.e., $\rho_{\rm da}(t) = {\rm Tr}\left\{U(t,0)\rho(0)U^{-1}(t,0)\right\}_{\rm B}$, $U(t,0)$ being the propagator of the full system plus bath. The bath is modelled by a collection of harmonic modes $H_{\rm B} = \frac{1}{2}\sum_\ell \left(p_\ell^2 + \omega_\ell^2 q_\ell^2\right)$ in thermal equilibrium at temperature T.

QUAPI is based on a symmetric Trotter splitting of the short-time propagator $\mathscr{K}(t_{k+1}, t_k)$ for the full Hamiltonian into a part depending on the system Hamiltonian and a part involving the bath and the coupling term[34,102,103]. The splitting of propagator in terms of the short-time propagator is, by construction, exact in the limit $\delta t = t_{k+1} - t_k \to 0$. However, for finite δt it introduces a finite Trotter error, which has to be eliminated by choosing δt small enough until convergence is achieved[34,102,103].

Another key ingredient in QUAPI's performance is the treatment of non-Markovian time evolution generated from the non-local correlations of the bath modes (see Sec. 2.4). For any finite temperature, these correlations decay exponentially fast at asymptotic times, thereby setting the associated memory time scale[34,102,103]. This fact allows for the introduction of an effective memory-time window $\tau_{\rm mem} = \kappa\delta t$, so it is assumed that the system dynamics have memory over κ slices of time. Over this time window, QUAPI defines an object called the reduced density tensor, which has to be iterated in order to propagate the reduced density matrix of the system. Within the memory time window, all correlations are included exactly over the finite memory time $\tau_{\rm mem}$ and can, in principle, be neglected for times beyond $\tau_{\rm mem}$. Then, the memory parameter κ has to be increased, until convergence is found. So, we have the requirement of decreasing δt while increasing κ in order to get convergent results: the two strategies naturally run counter to one another. However, convergent results can be obtained over a wide range of parameter regimes[34,102,103].

The efficiency and implementation of the QUAPI algorithm are based on the choice of the parameters κ and M (the number of basis states), e.g., the reduced density tensor is a complex array of size $M^{2\kappa+2}$. This limits its applicability to the case of model systems that are not too large. For the case of the donor-acceptor dimer system, $M = 2$, so with the standard hardware architectures one can choose $\kappa \lesssim 12 - 14$[51,106]. However, if one is interested in studying, e.g., the network of eight bacteriochlorophyll-*a* chromophores in the FMO complex within the two level system framework one has $M = 16$, so $\kappa \sim 3$. This relatively short memory window could be problematic if one is interested in using this approach in the context of electronic transfer, e.g., in semiconducting carbon nanotubes[107].

Although QUAPI is an iterative scheme, the truncation of the memory makes the simulations scale linearly with the propagation time; however, since at low temperatures the bath induced correlations decay only algebraically[54,108,109], this truncation limits the applicability of QUAPI to the finite temperature scenario[34,102,103]. In comparative studies[34,106], it has been shown that QUAPI is able to generate the correct time evolution of photosynthetic complexes in the range of parameters of interest, finite temperature, strong system-bath interaction and strong electronic coupling.

QUAPI was implemented by Nalbach *et al.* in Ref. 34 in order to include the spectral density given in Eq. (12) derived in Ref. 37. The result suggests that the use of this spectral density provides slightly smaller coherences lifetimes than those observed in the experiment[11], those calculated using the Ohmic spectral density in Eq. (13), and those based on a hybrid quantum/classical all atom calculation[35]. It would be interesting to analyze this case using other methodologies in order to understand the role of the vibrational high frequency modes (see Sec. 2.4.1) in the dynamics.

3.2.3 NIBA-based methods—In a series of papers, Cao *et al.*[33,110,111] have explored the efficiency of the energy transfer in light-harvesting systems using approaches such

the Haken-Strobl model (pure dephasing)[112], the generalized Bloch-Redfield equation (second-order cumulant expansion model[110,113]) and the non-interacting-blip approximation (NIBA)[56,60]. The Haken-Strobl model has been extensively discussed in the literature[18] and the generalized Bloch-Redfield approach shares the spirit of the Nakajima-Zwanzig equation discussed in Sec. 3.1, so we discuss here the NIBA approximation[56,60] only.

To understand the term *non-interacting blip*, we can appeal to the path integral formulation of the systems with a finite Hilbert space[56,60]. For simplicity we restrict the discussion to the case of a system with two levels. Time evolution of double-sided objects, like the density matrix, is performed by a pair of trajectories[56,101]. In the case of the two level systems, these trajectories are piecewise constant paths with sudden jumps between states, so we have four possible "positions", namely both trajectories visit the ground or excited state or one of them visits the ground state while the other one is the excited state and vice-versa. The two paths can be seen as a single path visiting the four configurations. A period of the path spent in the diagonal configuration (ground-ground or excited-excited) is called a *sojourn* while a period the path spends in an off-diagonal configuration is a *blip*[56,60]. The NIBA assumption is that the average time the system spends in a diagonal configuration is much larger than time it spends in an off-diagonal one. This assumption motivates setting (i) the sojourn-blip and (ii) the blip-blip correlations to zero; this leads to the non-interacting blip approximation. In the strict Ohmic case, i.e., in the scaling limit $\omega_c \to \infty$, assumption (i) is *exact*[56]; thus, the approximation enters, in this case, in neglecting the interblip interactions.

An alternate, apparently less complicated, approach to deriving the NIBA is given in Ref. 114.

According to Ref. 56, this approximation can be justified for:

1. Weak-coupling to the environment and zero bias.
2. Super-Ohmic spectral densities with $s > 1$ and $s > 2$ at zero and finite temperature, respectively.
3. Sub-Ohmic spectral densities with $s < 1$ and $s < 2$ at zero and finite temperature, respectively. Therefore, NIBA is justified[56,60] (i) at all temperature in the sub-Ohmic case, (ii) at high temperature in the Ohmic case, and (iii)at high temperatures in the super-Ohmic case with $s < 2$.[56,60].

NIBA can be formulated as a second-order master equation in the bath-dressed electronic coupling[115], which is more convenient for the extension to multilevel systems[33]. This strategy was followed in Ref. 33 to generate a version of NIBA for multi-state systems. This extended NIBA was compared to the generalized Bloch-Redfield approach by Cao *et al.*[33] for describing the time evolution of site populations in the FMO complex with eight bacteriochlorophyll-*a* chromophores; the results are in excellent qualitative agreement. NIBA's performance was also studied in Ref. 116 in a wide range of parameters. In the limits described above, it provides accurate results.

4 Molecular Modelling of Photosynthetic Complexes

Molecular modelling of photosynthetic complexes is of primary importance insofar as information about electronic couplings, site energies, spectral densities, linear absorption spectrum, etc. are obtained from such studies[20,37,40,117,118]. Recently, Mennucci and Curutchet[20] presented a complete perspective on these approaches and König and Neugebauer[22] reviewed the advantages and pitfalls of most of these theoretical methods in providing EET coupling constants. Here we review some of the most recent progress and physical insights from the molecular-modelling studies.

As described in Ref. 20, among the various proposals for molecular modelling one can distinguish two methodologies for describing the environment and its effects on screening the Coulomb interaction between the donor and acceptor transition dipoles. The first method considers the environment as a dielectric continuum. Its effects are characterized by means of a screening factor $1/n^2$, where n is the solvent refractive index (Förster-like theories). The second approach treats the environment at the atomic level, either by using molecular mechanics force fields or by incorporating a full quantum mechanical description of the chromophore-environment.

Mennucci *et al.* have developed a method, reliant upon the dielectric-continuum-based approach, using a combination of the quantum linear response and a structureless-polarizable-continuum-media model of the environment[20,119]. The method is able to deal with the non-equilibrium response of the system and of the environment during fast processes, such as those involved in electronic transitions and electronic energy transfer[20]. It has been successfully applied to examine the screening induced by the environment in the electronic couplings for a set of over 100 chromophore pairs, including chlorophylls, bilins and carotenoids, taken from structural models of photosynthetic pigmentprotein complexes[20,117]. An interesting outcome from this methodology is the fact that photosynthetic light-harvesting can be tuned by heterogeneous polarizable environments of the proteins[120] and that the final resonance energy transfer step could occur on a timescale of 15 ps. According to Ref. 120, such a rapid final energy transfer step cannot be reproduced by calculations based on the spectral density description, which predict the energy transfer times to be on the order of 40 ps[40].

The second method, where one carries out a quantum all-

atoms calculation for the structure and dynamics of photosynthetic complexes, is currently beyond computational reach. In order to overcome this problem, some methods based on quantum/classical[35,121–124] and continuum/atomistic descriptions have been proposed[20,125]. For a review of the main difficulties in the implementation of these approaches, such as the inclusion of the polarizability of the solvent and the heterogeneous character of the environment, the interested reader is referred to Refs. 20,22.

Apart from the difficulties in computing the various electric couplings using atomistic an description, a major challenge is the full-atom description of the dynamics itself. A first step towards an all-atom calculation of the dynamics of photosynthetic complexes, in particular of the FMO complex, was presented by Aspuru-Guzik *et al.* in Ref. 35. Based on the Born-Oppenheimer approximation and adopting the Condon approximation, they decomposed the total system Hamiltonian into three parts: a system Hamiltonian acting on the exciton sector (described by a set of two-level systems), a bath of vibrational modes, and a coupling term between them; this corresponds to the discussion in Sec. 2.2.2.2. The molecular energies are computed using time-dependent density functional theory with the dynamics done by the Wigner method, i.e. the exciton dynamics are done quantum mechanically and the bath dynamics are done classically. The evolution of the excitonic density matrix is obtained from a statistical ensemble of unitary evolutions obtained by solving a time-dependent Schrödinger equation. This approach allows consideration of nonidentical fluctuations across all the sites. The population dynamics of the chromophore is in accordance with previous calculations[18,77,84]. Based on this approach, Aspuru-Guzik *et al.*[35] concluded that the site energy cross-correlation between chromophores does not play a significant role in the energy transfer dynamics. This is in accord with the results of Olbrich in Refs. 123,124 for the FMO complex and with those of Huo and Coker[31] for the PC645 complex.

It is worth mentioning that the statistical-ensemble-averaging approach has inspired the application of quantum state diffusion approaches such as those discussed in Refs. 126,127. In particular, it has been used to study the role of quantum oscillations as well as the dependence on site energies in electronic excitation transfer in the FMO complex[128], the influence of the vibrational modes[129] and the influence of noise, disorder, and temperature on localization in excitonic systems[130]. These techniques appear accurate, efficient and are valid for a wide spectrum of parameters[128–130].

In addition, we note that direct connections are being established between all-atoms calculations and master equation approaches that use spectral densities[58,131]. For example, Ref. 58 obtained spectral densities associated with FMO by such a full-atom computation. Results, whose effect on FMO dynamics is yet to be determined, show structured $J(\omega)$ with considerably higher values of ω contributing to the spectral density than assumed in the Ohmic or Drude-Lorentz models or Adolphs-Renger model[37] previously utilized.

Finally, note that recent evidence has been found for correlated fluctuations of site energies and intersite electronic couplings as well as electronic-electronic coupling that could be more significant than the apparently uncorrelated site energy fluctuations[124,132] Hence, an interesting possible direction in this regard is to develop technique which provide spectral densities that include bath-dependent electronic terms[132].

5 Insights into the Observed Coherences

Below we discuss some of the issues relating to the role of the observed EET dynamics in natural photosynthetic processes, and introduce an analytic model that provides physical insight into the origins of the observed long-lived coherences.

5.1 Natural processes

We remark on two issues in need of considerable clarification if we are to understand the role of the observed coherences in nature. First, note that under natural conditions, photosynthetic complexes are excited by sunlight, an incoherent source of light[63–68] that is incident on the system for times that are huge compared to the time scale of the molecular dynamics. As a consequence, excitation of this kind cannot generate coherent dynamics among the pigments, neither in the case of the unitary dynamics associated with isolated molecules,[63,64,66,67] nor in the case of open systems, where the molecule is in contact with an environment[65,68]. Based on this argument, it is not yet clear whether coherences induced by coherent femtosecond laser pulses can play a role under *in vivo* conditions.

Second, there remains a concern that the observed coherences may not necessarily be solely electronic in nature, i.e., suggestions have been made that vibrational coherences are being observed as well (cf. Ref. 133). Only very recently has an experimental protocol been applied that, based on the nature of the observed 2D Photon Echo experiment, can distinguish between electronic and vibrational coherences. A recent application of this protocol[134] for the case of PC645 has identified one of the observed long-lived coherences as electronic, and the others as likely vibrational. In this regard we note that vibrational coherences would be expected to decohere slowly[135] so that understanding such a coherence feature presents no significant qualitative challenge.

5.2 The origin of long-lived coherences

The major part of this paper has provided a review of a number of techniques and approaches for the study of the EET dynamics of photosynthetic complexes. Examination of these

detailed computations shows, however, that they do not provide direct insight into the basic physical origin of the observed longevity of the coherences. Below we address the question as to the physical origin of the long-lived observed coherences, by introducing an analytically soluble model that provides correct results for dimers that characterize the FMO and PC645 systems.

At high temperatures and for weak coupling to the environment, a classical treatment of the thermal fluctuations with an Ohmic spectral density with exponential decay (see Sec. 2.4.1) predicts that the electronic coherence discussed in Sec. 2.2.2.1 decays at a *Gaussian* rate that can be determined as [15,136,137]

$$\tau_{\rm G} = \sqrt{\hbar^2/2\lambda k_{\rm B} T}, \tag{21}$$

where λ is the system reorganization energy. Based on this expression, the dephasing time for photosynthetic complexes, for a typical value of $\lambda = 130\ {\rm cm}^{-1}$), can be estimated [15] to be $\tau_{\rm G} = 45$ fs at $T = 77$ K and $\tau_{\rm G} = 23$ fs and $T = 294$ K.

By contrast, the experiments in photosynthetic complexes such as the FMO complex [11,14] and the PC645 complex [13], discussed above, have found that electronic coherences among different chromophores survive up to 800 fs at 77 K [11] and up 400 fs at room temperature [13]. Generally longer coherence times have been observed for FMO in Ref. 14. This surprising observation and its possible consequences for biological processes have been discussed extensively [11,13–15,27,28,31,34,35,84,110,138] and have provided motivation for the development of the methodologies discussed above. Interestingly, despite the diversity of approaches and techniques, most [13,15,16,28,31,34,35,84,138] predict long-lived coherences on the same time scales as those found experimentally [11,13,14]. This suggests that the underlying physical features are correctly contained in these approaches. However, the sheer complexity of these computations has limited one from identifying these essential physical features [16].

In order to explore the physical features responsible for the survival of these coherences, we (in Ref. 16) discuss the case of the relatively strongly coupled dimer composed of the BChl1*a* 1 and BChl1*a* 2 in the FMO complex (see Sec. 2.1), and the dimer formed of chromophores DVBc and DVBd in the PC645 complex (see also Sec. 2.1). The generic Hamiltonian for the two two-level system is described in terms of Pauli spin matrices by [59,61]

$$\begin{aligned} H = &\frac{\hbar}{2}\varepsilon_1\sigma_{z,1} + \frac{\hbar}{2}\varepsilon_2\sigma_{z,2} + \frac{\hbar}{2}\Delta(\sigma_{x,1}\sigma_{x,2} + \sigma_{y,1}\sigma_{y,2}) \\ &+ \frac{\hbar}{2}\delta\mu_1\sigma_{z,1}R_1 + \frac{\hbar}{2}\delta\mu_2\sigma_{z,2}R_2 + B_1 + B_2, \end{aligned} \tag{22}$$

where $R_i = \sum_\alpha C_{\alpha,i}\left(a_{\alpha,i} + a^\dagger_{\alpha,i}\right)$ is the reaction field operator for molecule i, $B_i = \sum_\alpha \hbar\omega_{\alpha,i} a^\dagger_{\alpha,i} a_{\alpha,i}$ is the energy stored in the solvent cage of molecule i and $\delta\mu_j$ is the difference between the dipole moment of the chromophore j in the ground and excited states [59,61]. The first two terms in Eq. (22) are the contributions from the individual sites and the third term is the Δ coupling between them. The subsequent terms describe the system-bath coupling. Following Refs. 61 and 116, the Hamiltonian in Eq. (22) can be written with respect to the basis $\{|g_1\rangle\otimes|g_2\rangle, |g_1\rangle\otimes|e_2\rangle, |e_1\rangle\otimes|g_2\rangle, |e_1\rangle\otimes|e_2\rangle\}$ describing the state of the two chromophores, i.e.

$$\begin{aligned} H = &\sum_{i=1,2}\sum_\alpha \hbar\omega_{\alpha,i} a^\dagger_{\alpha,i} a_{\alpha,i} \\ &+ \frac{\hbar}{2}\begin{pmatrix} -(\varepsilon_+ + V_+) & 0 & 0 & 0 \\ 0 & -(\varepsilon_- + V_-) & 2\Delta & 0 \\ 0 & 2\Delta & \varepsilon_- + V_- & 0 \\ 0 & 0 & 0 & \varepsilon_+ + V_+ \end{pmatrix}, \end{aligned}$$

where $\varepsilon_\pm \equiv \varepsilon_1 \pm \varepsilon_2$, and $V_\pm \equiv \delta\mu_1 R_1 \pm \delta\mu_2 R_2$.

Since under excitation by weak light only the singly excited states need to be taken into account, we can identify [61,116] the active environment coupled 2D-subspace as $\{|e_1\rangle\otimes|g_2\rangle, |g_1\rangle\otimes|e_2\rangle\}$. In this central subspace of Eq. (23), the effective interacting biomolecular two-level system Hamiltonian reads

$$H = \left(\frac{\hbar\varepsilon}{2}\sigma_z + \hbar\Delta\sigma_x\right) + \frac{\hbar}{2}\sigma_z V + \sum_{\substack{\alpha \\ i=1,2}} \hbar\omega_{\alpha,i} a^\dagger_{\alpha,i} a_{\alpha,i} \tag{23}$$

where $\varepsilon \equiv \varepsilon_-$ and $V \equiv V_-$. This is schematically illustrated in Fig. 1, where Δ is the associated "tunneling energy", between the new basis states $|e_1\rangle\otimes|g_2\rangle$ and $|g_1\rangle\otimes|e_2\rangle$.

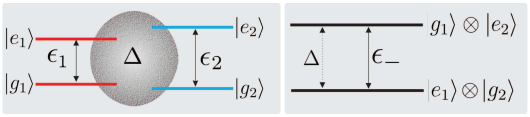

Fig. 1 Left hand side: The pair of interacting chromophores. Right hand side: the effective light harvesting two-level system formed from the pair of interacting chromophores [61,116].

Following the description given in Sec. 2.2, we assume that the two baths are uncorrelated $\langle R_1(t'')R_2(t')\rangle = \langle R_2(t'')R_1(t')\rangle = 0$. Hence, Eq, (23) can be written in the standard form of the spin-boson model [61]

$$H = \left(\frac{\hbar\varepsilon}{2}\sigma_z + \hbar\Delta\sigma_x\right) + \frac{\hbar}{2}\sigma_z\sum_\beta g_\beta(b_\beta + b^\dagger_\beta) + \sum_\beta \hbar\omega_\beta b^\dagger_\beta b_\beta\ , \tag{24}$$

where the b_β includes harmonic oscillators coupled to both chromophores, with couplings g_β. The effects of the baths are treated in terms of the Ohmic spectral density with exponential decay presented in Sec. 2.4.1.

The Hamiltonian in Eq. (24) differs from the one described in Sec. 2.2.2.2 by the fact that in Eq. (24), both states $|e_1\rangle \otimes |g_2\rangle$ and $|g_1\rangle \otimes |e_2\rangle$ are coupled to the same effective bath modes, whereas the treatment presented in Sec. 2.2.2.2 shows that for the case of a pair of donor-acceptor pigments, the ground and excited states should be coupled to independent modes. Although, this fact introduces fluctuations of the reference energy of the donor-acceptor system, if one is interested only in the dynamics of the Bloch oscillation this is irrelevant (cf. Ref. 51,59). For strong coupling to the bath or high degree of non-Markovian dynamics, one expects the two models, e.g, are driven to different thermal states. However, the fact that our results, see below, coincide with the overwhelming majority of the current results in literature, means that the coupling strength and the degree of non-Markovian character, for the particular cases discussed below, are still in a regime where both models coincide. Note also that the previous predictions made for the lifetimes (cf. Ref. 15) were based on the spin boson-model. Thus, in order to get an idea about the lifetimes of the coherences, the model is quite well justified.

The parameter range within which the dimers described above, BChl1*a* 1 and BChl1*a* 2 in the FMO complex and the chromophores DVBc and DVBd in the PC645 complex, lie allows for the use of the non-Markovian NIBA plus first order corrections in the interblip correlation strength, i.e. an *enhanced NIBA approximation*. For a description of the range of applicability of the *bare* NIBA cf. Sec. 3.2.3. The enhanced approximation is valid for weak system-bath coupling and for $\varepsilon/2\Delta < 1$, over the whole range of temperatures (see Chap. 21 in Ref. 56), and provides simple and accurate *analytic* expressions for relaxation and decoherence rates. As it was discussed

K	$\varepsilon/2\Delta$	$k_{\rm B}T/2\hbar\Delta$	$2\Delta/\omega_{\rm c}$	$k_{\rm B}T/\hbar\omega_{\rm c}$	$\varepsilon/\omega_{\rm c}$
0.105	0.428	0.305	1.052	0.321	0.45
0.105	0.428	1.098	1.052	1.154	0.45

Table 1 Parameters used for dimer formed of BChl*a* 1 and BChl*a* 2 at $T = 77$ K (first row) and $T = 277$ K (second row).

in Sec. 3.2.3, in the limit when $\omega_{\rm c}$ is much larger than the other frequencies in the system, NIBA is exact. In the present case, see Table 1, this condition is not fulfilled in all cases; however, we do have here an improved approximation which provides lifetime estimates that are in very good agreement with experimental as well more-refined-theoretical results.

The high temperature limit in this approach is given by temperatures well in excess of $T_{\rm b} = \hbar(\Delta_{\rm eff}^2 + \varepsilon^2)^{1/2}/k_{\rm B}$, where

$$\Delta_{\rm eff} = [\Gamma(1-2K)\cos(\pi K)]^{1/2(1-K)}(\tilde{\Delta}/\omega_{\rm c})^{K/(1-K)}\tilde{\Delta},$$

where in our case $\tilde{\Delta} = 2\Delta$. Here the spectral density is ohmic [Eq. (14)] where K describes the coupling strength to the bath and $\omega_{\rm c}$ is the bath cutoff frequency.

For the set of parameters listed in Table 1, we find $T_{\rm b} \approx 288$ K. Hence the FMO experiments, at 77 K and 277 K, are in the low temperature regime, $T < T_{\rm b}$. In this regime, the Rabi frequency Ω, the relaxation rate $\gamma_{\rm r}$ and the decoherence rate γ are given by[56]

$$\Omega^2 = \Delta_{\rm b}^2 + 2K\Delta_{\rm eff}^2\,[\Re\psi(i\hbar\Delta_{\rm b}/2\pi k_{\rm B}T) - \ln(\hbar\Delta_{\rm b}/2\pi k_{\rm B}T)] \quad (25)$$

$$\gamma_{\rm r} = \pi K \coth(\hbar\Delta_{\rm b}/2k_{\rm B}T)\Delta_{\rm eff}^2/\Delta_{\rm b}, \quad (26)$$

$$\gamma = \gamma_{\rm r}/2 + 2\pi K(\varepsilon^2/\Delta_{\rm b}^2)k_{\rm B}T/\hbar, \quad (27)$$

respectively, where $\Delta_{\rm b} = \sqrt{\Delta_{\rm eff}^2 + \varepsilon^2}$ and $\psi(z)$ is the digamma function. (Note that in Refs. 139 and 56, the term $\Delta_{\rm eff}^2$ is missing in the expression for Ω.) The expressions in Eqs. (25)-(27) were derived for the particular case of non-Markovian Ohmic dissipation, however, analogous expressions for arbitrary spectral densities can be found in Refs. 16,56,139.

Based on this model, and using the parameters in Table 1 (obtained from experimental results[16]), we find[16] the following time scales for the FMO complex $2\pi\Omega^{-1} = 163$ fs, $\gamma_{\rm r}^{-1} = 90$ fs, $\gamma^{-1} = 153$ fs at $T = 77$ K, while $2\pi\Omega^{-1} = 151$ fs, $\gamma_{\rm r}^{-1} = 45$ fs, $\gamma^{-1} = 69$ fs at $T = 277$ K. For the case the dimer formed of chromophores DVBc and DVBd in the PC645 complex, we predicted $2\pi\Omega^{-1} = 49$ fs, $\gamma_{\rm r}^{-1} = 76$ fs and $\gamma^{-1} = 88$ fs at $T = 294$ K using the parameters in Refs. 16,29,40. Note that $\gamma_{\rm r}^{-1}$ and γ^{-1} are related to decay rates and that the time period over which coherence is observed is therefore much longer[16]. For example, electronic coherences are observed to persist in PC645 at room temperature for times up to 400 fs, a result predicted by this model as well. Similarly, the time scales over which coherences persist for FMO, predicted from this model, are in agreement with all other (far more complex) computations, and with the earlier experimental results in Ref. 11.

Hence, the long time scales seen to emerge naturally here from the system parameters. Why then were far shorter decoherence time scales originally expected for these systems? To see this, note that in molecular systems, dynamics is often studied between different electronic eigenstates of the system, separated by greater than $\sim 10^4$ cm^{-1}, with no coupling between them. In such cases, the dephasing time from Eqs. (26) and Eq. (27) would be extremely short. By contrast, in the case of photosynthetic complexes, energy transfer occurs between exciton states that are close in energy and, additionally, are coupled. This generates a small value for the ratio $\varepsilon/2\Delta$ which in turn is responsible for longer dephasing times (see Fig. 2).

Additionally, expressions such as $\tau_{\rm G}$ [Eq. (21)], which are often used to estimate rates, are only valid at high temperature, $k_{\rm B}T \gg \hbar\omega_{\rm c}$, and at short times, $t < \omega_{\rm c}^{-1}$. Under conditions

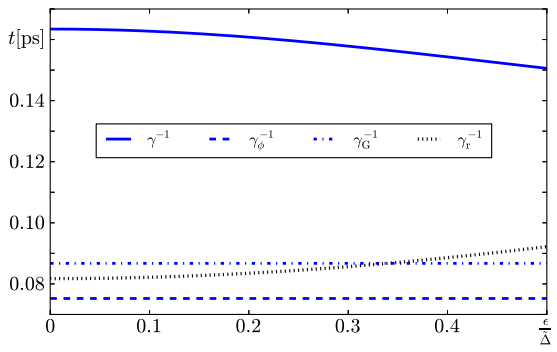

Fig. 2 Decoherence time γ^{-1} (continuous blue line) as functions of $\varepsilon/2\Delta$, for fixed $\Delta = 35$ cm^{-1} and at $T = 77$ K. The dashed blue line denotes the dephasing rate used in Refs. 14,28,137 given by $\gamma_\phi = 2\pi(k_B T/\hbar)\lambda/\hbar\omega_c$ while the dotdashed blue line denotes the decoherence time $\tau_G = \sqrt{\hbar^2/2\lambda k_B T}$ used in references 15,136,137. The relaxation time γ_r^{-1} is depicted by the black dotted line. Fixed parameters as in Table 1. The data for this plot was taken from Ref. 16. Note that color is oniine, but not in the printed text.

when the expression for τ_G is valid, the bath modes can be treated classically [140], as in Refs. 45 and 46. When one is not in the appropriate regime, the classical evolution of the bath underestimates quantum coherence effects [140] because at low temperatures quantum fluctuations overcome thermal fluctuations [136]. Hence, estimates based on τ_G in Eq. (21) are unreliable. Moreover, as we already mentioned, τ_G characterizes a Gaussian decay, while in the experimental results [11,13,14] the decay is observed to be exponential.

Similarly, the expression $\gamma_\phi = 2\pi(k_B T/\hbar)\lambda/\hbar\omega_c$, another usual expression for estimating the exponential decay at high temperature, also provides an inadequate representation of the true physics and associated dependence on system and bath parameters. This expression is derived in the limit $\varepsilon \to 0, K \to 0$ and $\omega_c \to \infty$, so it is expected to result in decoherence times that are underestimated and misleading [16].

In Fig. 2, we have shown the explicit dependence of the various decay rates in Eqs. (25)-(27) for fixed values of the ratio $\varepsilon/2\Delta$ using the FMO parameters at 77 K. We observe that the decay rate increases for large values of this ratio. Based on this result and our previous discussion, one can identify three physical features found to be responsible for long coherence lifetimes: (i) *the small energy gap between excitonic states* (ii) *the small ratio of the energy gap to the coupling between excitonic states*, and (iii) *the fact that the molecular characteristics place the system in an effective low temperature regime, even at ambient conditions.*

In this framework, the observed long lifetimes arise naturally and are not surprisingly long. This physical picture described above, was subsequently verified by Cao *et al.* [33] using the Hamiltonian described in Sec. 2.2.2.2. A similar physical picture for the survival of coherences has emerged independently in other physical systems such as spin charge qubits in quantum dots [141,142] or in electronic excitations in semiconducting carbon nanotubes [107]. This provides some robustness to the findings in Ref. 16.

5.3 Coherences and energy transfer

The possibility that the coherences observed in the 2D electronic spectroscopy experiments [10–14] could be assisting the high efficiency of the photosynthetic process has been one of the more exciting conjectures in the field. However, there is now sufficient theoretical evidence from different groups, such as Whaley *et al.* [143], Olbrich *et al.* [35,123], Cao *et al.* [33,110,111], Coker *et al.* [31] and Aspuru-Guzik *et al.* [35], suggest that the presence of these coherences has only a slight effect on energy transfer.

6 Some Future Directions

Results discussed above apply to the specific case of EET in photosynthetic light harvesting. We remark on a number of possible related extensions of interest.

1. It is worth noting a critical and interesting overview on EET modelling in light-harvesting complexes by Huo and Coker in Ref. 31. They point out that despite the complexity, diversity and variability of the protein-pigment complexes (see Sec. 2.1), all of these complexes are highly efficient and the Hamiltonians of these systems, parametrized using the molecular modelling methodologies discussed in Sec. 4, share some generic features [31]: (i) *Clusters of chromophores with closely spaced excitation energies that have appreciable electronic couplings between the cluster members.* (ii) *Chromophore states whose excitation energies are isolated, but which exhibit appreciable electronic coupling to neighboring states.* (iii) *These isolated but coupled states are often arranged energetically in cascade or barrier patterns that channel the directional flow of energy through these multichromophore networks, and toward reaction centers.*

These features, and those discussed in Sec. 5.2, could be used as the target properties for artificially designed light-harvesting complexes. These characteristics could be the desirable outcome of molecular designs based on current or new molecular modelling strategies, such as those described in Sec. 4. Work in this direction is worth considering, mainly because it would relate the studies above to the ultimate goal of designing artificial light-harvesting devices inspired by nature, and currently of great interest (e.g., Ref. 144) .

2. The physical insights discussed in Sec. 5.2 describe how coherence can be preserved after a single photon excitation. Recently, motivated by possible natural scenarios such as photo-protection[8], there is interest in the possibility that the observed coherence can be restored continuously in time[145]. This situation suggests a role for non-equilibrium phenomena in EET.

The importance of non-equilibrium contributions can be examined in terms of the results derived, in a different context, by Pachón *et al.* in Ref. 146. They have shown that for out-of-equilibrium quantum systems, the border between the classical and the quantum realms is more intricate than that for the equilibrium situation. In particular, they have shown that some quantum features, such as entanglement, can survive under higher temperatures in non-equilibrium cases than in the equilibrium case[146] (see also Ref. 147). However, even if the process described in Ref. 146 could protect the coherences, it is not clear whether or not they could optimize EET, even though preliminary results show that these coherence could be spatially directing energy transfer[145].

3. The results described above show that the notion of a "high temperature regime" is relative, it depends on the energetics of the complex and as well as on the solvent properties. That is, room temperature could be low temperature for some systems but high temperature for others. The fact that EET in photosynthetic complexes relies on the moderate/low temperature can be seen to be a way of protecting the possible coherent dynamics that could take place in the light harvesting process. The reason for this is that, at low temperatures and in the long time regime, the decay of the correlations is expected to be algebraic, $1/t^2$, rather than exponential, $\exp(-\gamma_m t)$,[54,108,109]. Thus, in the low temperature regime the coherences are expected to decay more slowly than in the high temperature regime. Our discussion in Sec. 5.2 offers the basis for exploring the design or the search of natural complexes in an effective low temperature, where the electronic coherences could live even longer than seen at present.

4. Although methodologies such as QUAPI[34,105,106] or the second order cumulant expansion[18,77,84] have provided valuable insights into EET, we call attention to some other promising new methodologies based on their reliability over a wide spectrum of parameters, their performance, and efficiency. They are also versatile, applying to different kinds of coupling terms and spectral densities. Specifically, we are referring to methodologies such PLDM (cf. Sec. 3.2.1) and those[128–130] based on quantum state diffusion[126,127] that are worth considering beyond the context of EET in photosynthetic complexes, e.g., in superconducting carbon nanotubes[107] or other physical solid-state physics systems[1–4]. After completing this Perspective, we noted the current interest in applying and developing efficient methodologies based on density-matrix renormalization-group approaches (cf. Ref 148,149), which seem to be highly efficient and could be used to explore possible mechanisms assisting EET in regions of the parameter space beyond the scope of our analysis (cf. Ref. 150) or with highly structured spectral densities.

Acknowledgments

We acknowledge helpful comments on this manuscript by Dr. Torsten Scholak, and by Professors David F. Coker and Gregory D. Scholes. This work was supported by the US Air Force Office of Scientific Research under contract number FA9550-10-1-0260 and by *Comité para el Desarrollo de la Investigación* –CODI– of Universidad de Antioquia, Colombia.

References

1 J. Jortner, S. A. Rice and R. Silbey, in *Excitons and Energy Transfer in Molecular Crystals*, ed. O. Sinanoglu, Academic Press, New York, 1965, p. 139.
2 A. Gedanken, J. Jortner, B. Raz and A. Szöke, *J. Chem. Phys.*, 1972, **57**, 3456–3469.
3 N. Schwentner, E.-E. Koch and J. Jortner, *Electronic Excitations in Condensed Rare Gases*, Springer Verlag, Berlin-Heidelberg-New York, 1985, vol. 107.
4 J. Moll, S. Daehne, J. R. Durrant and D. A. Wiersma, *J. Chem. Phys.*, 1995, **102**, 6362–6370.
5 T. Renger, V. May and O. Kühn, *Phys. Rep.*, 2001, **343**, 137 – 254.
6 V. May and O. Kühn, *Charge and energy transfer dynamics in molecular systems*, Wiley-VCH, Weinheim, 3rd edn, 2011.
7 V. Sundström, T. Pullerits and R. van Grondelle, *J. Phys. Chem. B*, 1999, **103**, 2327–2346.
8 H. van Amerongen, L. Valkunas and R. van Grondelle, *Photosynthetic Excitons*, World Scientific, Singapore, 2000.
9 J. M. Salverda, M. Vengris, B. P. Krueger, G. D. Scholes, A. R. Czarnoleski, V. Novoderezhkin, H. van Amerongen and R. van Grondelle, *Biophys. J.*, 2003, **84**, 450–465.
10 H. Lee, Y.-C. Cheng and G. R. Fleming, *Science*, 2007, **316**, 1462–1465.
11 G. S. Engel, T. R. Calhoun, E. L. Read, T.-K. Ahn, T. Mančal, Y.-C. Cheng, R. E. Blankenship and G. R. Fleming, *Nature*, 2007, **446**, 782–786.
12 I. P. Mercer, Y. C. El-Taha, N. Kajumba, J. P. Marangos, J. W. G. Tisch, M. Gabrielsen, R. J. Cogdell, E. Springate and E. Turcu, *Phys. Rev. Lett.*, 2009, **102**, 057402.
13 E. Collini, C. Y. Wong, K. E. Wilk, P. M. G. Curmi, P. Brumer and G. D. Scholes, *Nature*, 2010, **463**, 644–647.
14 G. Panitchayangkoon, D. Hayes, K. A. Fransted, J. R. Carama, E. Harel, J. Wen, R. E. Blankenship and G. S. Engel, *Proc. Natl. Acad. Sci. USA*, 2010, **107**, 12766–12770.
15 Y.-C. Cheng and G. R. Fleming, *Ann. Rev. Phys. Chem.*, 2009, **60**, 241–262.
16 L. A. Pachón and P. Brumer, *J. Phys. Chem. Lett.*, 2011, **2**, 2728–2732.
17 V. I. Novoderezhkin and R. van Grondelle, *Phys. Chem. Chem. Phys.*, 2010, **12**, 7352–7365.
18 A. Ishizaki, T. R. Calhoun, G. S. Schlau-Cohen and G. R. Fleming, *Phys. Chem. Chem. Phys.*, 2010, **12**, 7319–7337.
19 A. Olaya-Castro and G. D. Scholes, *Internatl. Rev. Phys. Chem.*, 2011, **30**, 49–77.

20 B. Mennucci and C. Curutchet, *Phys. Chem. Chem. Phys.*, 2011, **13**, 11538–11550.
21 G. S. Schlau-Cohen, A. Ishizaki and G. R. Fleming, *Chem. Phys.*, 2011, **386**, 1 – 22.
22 C. König and J. Neugebauer, *ChemPhysChem.*, 2012, **13**, 386–425.
23 Th. Förster, *Annalen der Physik*, 1948, **437**, 55–75.
24 Th. Förster, in *Delocalized excitation and excitation transfer*, ed. O. Sinanoglu, Academic Press, New York, 1965, p. 93.
25 A. G. Redfield, *IBM J. Res. Dev.*, 1957, **1**, 19–31.
26 A. Olaya-Castro, C. F. Lee, F. F. Olsen and N. F. Johnson, *Phys. Rev. B*, 2008, **78**, 085115.
27 M. B. Plenio and S. F. Huelga, *New J. Phys.*, 2008, **10**, 113019.
28 P. Rebentrost, M. Mohseni, I. Kassal, S. Lloyd and A. Aspuru-Guzik, *New J. Phys.*, 2009, **11**, 033003.
29 P. Huo and D. F. Coker, *J. Chem. Phys.*, 2010, **133**, 184108.
30 G. Tao and W. H. Miller, *J. Phys. Chem. Lett.*, 2010, **1**, 891–894.
31 P. Huo and D. F. Coker, *J. Phys. Chem. Lett.*, 2011, **2**, 825–833.
32 P. Huo and D. F. Coker, *J. Chem. Phys.*, 2011, **135**, 201101.
33 J. Moix, J. Wu, P. Huo, D. Coker and J. Cao, *J. Phys. Chem. Lett.*, 2011, **2**, 3045–3052.
34 P. Nalbach, D. Braun and M. Thorwart, *Phys. Rev. E*, 2011, **84**, 041926.
35 S. Shim, P. Rebentrost, S. Valleau and A. Aspuru-Guzik, *Boiphys. J.*, **102**, 649–660.
36 G. D. Scholes, *The Journal of Physical Chemistry Letters*, 2010, **1**, 2–8.
37 J. Adolphs and T. Renger, *Biophys. J.*, 2006, **91**, 2778–2797.
38 D. Tronrud, J. Wen, L. Gay and R. Blankenship, *Photosynth. Res.*, 2009, **100**, 79–87.
39 M. Schmidt am Busch, F. Müh, M. El-Amine Madjet and T. Renger, *J. Phys. Chem. Lett.*, 2011, **2**, 93–98.
40 T. Mirkovic, A. B. Doust, J. Kim, K. E. Wilk, C. Curutchet, B. Mennucci, R. Cammi, P. M. G. Curmi and G. D. Scholes, *Photochem. Photobiol. Sci.*, 2007, **6"**, 964–975.
41 M. A. Ratner, *J. Phys. Chem.*, 1990, **94**, 4877–4883.
42 O. V. Prezhdo and P. J. Rossky, *J. Chem. Phys.*, 1997, **107**, 5863–5878.
43 O. V. Prezhdo and P. J. Rossky, *Phys. Rev. Lett.*, 1998, **81**, 5294–5297.
44 M. Shapiro and P. Brumer, *Quantum Control of Molecular Processes*, Wiley-VCH, Weinheim, 2nd edn, 2011.
45 H. Hwang and P. J. Rossky, *J. Phys. Chem. B*, 2004, **108**, 6723–6732.
46 I. Franco and P. Brumer, *J. Chem. Phys.*, 2008, **128**, 244905.
47 I. Franco and P. Brumer, 2011, arXiv:1111.6461v1.
48 M. Schlosshauer, *Decoherence and the Quantum-To-Classical Transition*, Springer-Verlag, Berlin, 2007.
49 A. Nazir, *Phys. Rev. Lett.*, 2009, **103**, 146404.
50 F. Fassioli, A. Nazir and A. Olaya-Castro, *J. Phys. Chem. Lett.*, 2010, **1**, 2139–2143.
51 P. Nalbach, J. Eckel and M. Thorwart, *New J. Phys.*, 2010, **12**, 065043.
52 J. Strümpfer and K. Schulten, *J. Chem. Phys.*, 2011, **134**, 095102.
53 A. O. Caldeira and A. L. Leggett, *Physica A*, 1983, **121**, 587.
54 H. Grabert, P. Schramm and G. L. Ingold, *Phys. Rep.*, 1988, **168**, 115.
55 G.-L. Ingold, *Coherent Evolution in Noisy Environments*, Springer Verlag, Berlin-Heidelberg-New York, 2002, vol. 611.
56 U. Weiss, *Quantum Dissipative Systems*, World Scientific, Singapore, 3rd edn, 2008.
57 S. Mukamel, *Principles of Nonlinear Optical Spectroscopy*, Oxford University Press, New York, 1999.
58 C. Olbrich, J. Strümpfer, K. Schulten and U. Kleinekathöfer, *J. Phys. Chem. Lett.*, 2011, **2**, 1771–1776.
59 J. B. Gilmore and R. H. McKenzie, *J. Phys. Condens. Matter*, 2005, **17**, 1735–1746.
60 A. J. Leggett, S. Chakravarty, A. T. Dorsey, M. P. A. Fisher, A. Garg and W. Zwerger, *Rev. Mod. Phys.*, 1987, **59**, 1–85.
61 J. B. Gilmore and R. H. McKenzie, *Chem. Phys. Lett.*, 2006, **421**, 266.
62 A. Nemeth, F. Milota, T. Mančal, V. Lukeš, H. F. Kauffmann and J. Sperling, *Chem. Phys. Lett.*, 2008, **459**, 94 – 99.
63 X.-P. Jiang and P. Brumer, *J. Chem. Phys.*, 1991, **94**, 5833.
64 H. Hoki and P. Brumer, *Chem. Phys. Lett.*, 2009, **468**, 27.
65 T. Mančal and L. Valkunas, *New J. Phys.*, 2010, **12**, 065044.
66 H. Hoki and P. Brumer, *Procedia Chem.*, 2011, **3**, 122.
67 P. Brumer and M. Shapiro, *Molecular Response in One Photon Absorption: Coherent Pulsed Laser vs. Thermal Incoherent Source*, 2011, arXiv:1109.0026v2.
68 L. A. Pachón and P. Brumer, *Incoherent Excitation of Open Quantum Systems*, 2012, arXiv:.
69 G. W. Ford, J. T. Lewis and R. F. O'Connell, *Phys. Rev. Lett.*, 1985, **55**, 2273.
70 G. W. Ford, J. T. Lewis and R. F. O'Connell, *Phys. Rev. A*, 1987, **36**, 1466.
71 G. W. Ford, J. T. Lewis and R. F. O'Connell, *Phys. Rev. A*, 1988, **37**, 4419.
72 P. M. V. B. Barone and A. O. Caldeira, *Phys. Rev. A*, 1991, **43**, 57.
73 G. W. Ford and R. F. O'Connell, *Phys. Rev. A*, 1998, **57**, 3112.
74 G. Lindblad, *Commun. Math. Phys.*, 1976, **48**, 119.
75 V. Gorini, A. Frigerio, M. Verri, A. Kossakowski and E. C. G. Sudarshan, *Rep. Math. Phys.*, 1978, **13**, 149.
76 Y. C. Cheng and R. J. Silbey, *J. Phys. Chem. B*, 2005, **109**, 21399–21405.
77 A. Ishizaki and G. R. Fleming, *J. Chem. Phys.*, 2009, **130**, 234111.
78 S. Jang, M. D. Newton and R. J. Silbey, *Phys. Rev. Lett.*, 2004, **92**, 218301.
79 G. R. Fleming and M. Cho, *Ann. Rev. Phys. Chem.*, 1996, **47**, 109–134.
80 H.-P. Breuer, E.-M. Laine and J. Piilo, *Phys. Rev. Lett.*, 2009, **103**, 210401.
81 A. Rivas, S. F. Huelga and M. B. Plenio, *Phys. Rev. Lett.*, 2010, **105**, 050403.
82 L. A. Pachón and P. Brumer, 2012, In preparation.
83 H.-P. Breuer and F. Petruccione, *The Theory of Open Quantum Systems*, Oxford University Press, Oxford, 2002.
84 A. Ishizaki and G. R. Fleming, *Proc. Natl. Acad. Sci. USA*, 2009, **106**, 17255–17260.
85 S. Nakajima, *Progr. Theor. Phys.*, 1958, **20**, 948–959.
86 R. Zwanzig, *J. Chem. Phys.*, 1960, **33**, 1338–1341.
87 R. Zwanzig, *Phys. Rev.*, 1961, **124**, 983–992.
88 H. Grabert, *Projection Operator Techniques in Nonequilibrium Statistical Mechanics*, Springer Verlag, Berlin-Heidelberg-New York, 1982, vol. 95.
89 N. Singh and P. Brumer, *Faraday Discuss.*, 2011, **153**, 41–50.
90 F. Shibata and T. Arimitsu, *J. Phys. Soc. Jap.*, 1980, **49**, 891–897.
91 G. Ritschel, J. Roden, W. T. Strunz and A. Eisfeld, *New J. Phys.*, 2011, **13**, 113034.
92 J. Zhu, S. Kais, P. Rebentrost and A. Aspuru-Guzik, *J. Phys. Chem. B*, 2011, **115**, 1531–1537.
93 H.-D. Meyera and W. H. Miller, *J. Chem. Phys.*, 1979, **70**, 3214–3223.
94 G. Stock and M. Thoss, *Phys. Rev. Lett.*, 1997, **78**, 578–581.
95 M. Thoss and G. Stock, *Phys. Rev. A*, 1999, **59**, 64–79.
96 S. Bonella, D. Montemayor and D. F. Coker, *Proc. Natl. Acad. Sci. USA*, 2005, **102**, 6715–6719.
97 S. Bonella and D. F. Coker, *J. Chem. Phys.*, 2005, **122**, 194102.
98 E. R. Dunkel, S. Bonella and D. F. Coker, *J. Chem. Phys.*, 2008, **129**, 114106.
99 T. Dittrich and L. A. Pachón, *Phys. Rev. Lett.*, 2009, **102**, 150401.
100 T. Dittrich, E. A. Gómez and L. A. Pachón, *J. Chem. Phys.*, 2010, **132**, 214102.
101 L. A. Pachón, G.-L. Ingold and T. Dittrich, *Chem. Phys.*, 2010, **375**, 209

– 215.
102 N. Makri and D. E. Makarov, *J. Chem. Phys.*, 1995, **102**, 4600–4610.
103 N. Makri and D. E. Makarov, *J. Chem. Phys.*, 1995, **102**, 4611–4618.
104 M. Thorwart, *Tunneling and vibrational relaxation in driven multilevel systems in driven multilevel systems*, Shaker Verlag, 2000.
105 M. Thorwart, J. Eckel, J. Reina, P. Nalbach and S. Weiss, *Chem. Phys. Lett.*, 2009, **478**, 234 – 237.
106 P. Nalbach, A. Ishizaki, G. R. Fleming and M. Thorwart, *New J. Phys.*, 2011, **13**, 063040.
107 R. Hanson, L. P. Kouwenhoven, J. R. Petta, S. Tarucha and L. M. K. Vandersypen, *Rev. Mod. Phys.*, 2007, **79**, 1217–1265.
108 H. Grabert, U. Weiss and P. Talkner, *Z. Phys. B*, 1984, **55**, 87.
109 F. Haake and R. Reibold, *Phys. Rev. A*, 1985, **32**, 2462–2475.
110 J. Wu, F. Liu, Y. Shen, J. Cao and R. J. Silbey, *New J. Phys.*, 2010, **12**, 105012.
111 F. Wu, J.and Liu, J. Ma, X. Wang, R. Silbey and J. Cao, 2011, arXiv:1109.5769.
112 H. Haken and G. Strobl, *Z. Phys. A Hadron Nucl.*, 1973, **262**, 135–148.
113 J. Cao, *J. Chem. Phys.*, 1997, **107**, 3204–3209.
114 H. Dekker, *Phys. Rev. A*, 1987, **35**, 1436–1437.
115 C. Aslangul, N. Pottier and D. Saint-James, *J. Phys. France*, 1986, **47**, 1657–1661.
116 J. Eckel, J. H. Reina and M. Thorwart, *New J. Phys.*, 2009, **11**, 085001.
117 G. D. Scholes, C. Curutchet, B. Mennucci, R. Cammi and J. Tomasi, *J. Phys. Chem. B*, 2007, **111**, 6978–6982.
118 Y. Jing, R. Zheng, H.-X. Li and Q. Shi, *The Journal of Physical Chemistry B*, 2012, **116**, 1164–1171.
119 J. Tomasi, B. Mennucci and R. Cammi, *Chem. Rev.*, 2005, **105**, 2999–3094.
120 C. Curutchet, J. Kongsted, A. Muñoz Losa, H. Hossein-Nejad, G. D. Scholes and B. Mennucci, *J. Am. Chem. Soc.*, 2011, **133**, 3078–3084.
121 A. Damjanović, I. Kosztin, U. Kleinekathöfer and K. Schulten, *Phys. Rev. E*, 2002, **65**, 031919.
122 C. Curutchet, A. Muñoz Losa, S. Monti, J. Kongsted, G. D. Scholes and B. Mennucci, *J. Chem. Theory Comput.*, 2009, **5**, 1838–1848.
123 C. Olbrich and U. Kleinekathöfer, *J. Phys. Chem. B*, 2010, **114**, 12427–12437.
124 C. Olbrich, J. Strümpfer, K. Schulten and U. Kleinekathöfer, *J. Phys. Chem. B*, 2011, **115**, 758–764.
125 F. Müh, M. E.-A. Madjet, J. Adolphs, A. Abdurahman, B. Rabenstein, H. Ishikita, E.-W. Knapp and T. Renger, *Proc. Natl. Acad. Sci. USA*, 2007, **104**, 16862–16867.
126 T. Yu, L. Diósi, N. Gisin and W. T. Strunz, *Phys. Rev. A*, 1999, **60**, 91–103.
127 J. T. Stockburger and H. Grabert, *Phys. Rev. Lett.*, 2002, **88**, 170407.
128 G. Ritschel, J. Roden, W. T. Strunz, A. Aspuru-Guzik and A. Eisfeld, *J. Phys. Chem. Lett.*, 2011, **2**, 2912–2917.
129 G. Ritschel, J. Roden, W. T. Strunz and A. Eisfeld, *New J. Phys.*, 2011, **13**, 113034.
130 J. M. Moix, Y. Zhao and J. Cao, *arXiv:1202.4705v1*, 2012.
131 C. Olbrich and U. Kleinekathöfer, *J. Phys. Chem. B*, 2010, **114**, 12427–12437.
132 H. Pengfei and D. F. Coker, *J. Chem. Phys.*, 2012, **130**,.
133 N. Christensson, H. F. Kauffmann, T. Pullerits and T. Mancal, *arXiv:1201.6325v1*, 2012.
134 D. B. Turner, R. Dinshaw, K.-k. Lee, M. Belsley, K. E. Wilk, P. M. G. Curmi and G. Scholes, *Phys. Chem. Chem. Phys.*, 2012, –.
135 Y. Elran and P. Brumer, *J. Chem. Phys.*, 2004, **121**, 2673–2684.
136 H. Hwang and P. J. Rossky, *J. Chem. Phys.*, 2004, **120**, 11380.
137 J. B. Gilmore and R. H. McKenzie, *J. Phys. Chem. A*, 2008, **112**, 2162–2176.
138 J. S. Briggs and A. Eisfeld, *Phys. Rev. E*, 2011, **83**, 051911.
139 U. Weiss and M. Wollensak, *Phys. Rev. Lett.*, 1989, **62**, 1663.
140 M. Thoss, H. Wang and W. H. Miller, *J. Chem. Phys.*, 2001, **115**, 2991.
141 J. R. Petta, A. C. Johnson, J. M. Taylor, E. A. Laird, A. Yacoby, M. D. Lukin, C. M. Marcus, M. P. Hanson and A. C. Gossard, *Science*, 2005, **309**, 2180–2184.
142 B. F. Habenicht, H. Kamisaka, K. Yamashita and O. V. Prezhdo, *Nano Lett.*, 2007, **7**, 3260–3265.
143 S. Hoyer, M. Sarovar and K. B. Whaley, *New J. Phys.*, 2010, **12**, 065041.
144 R. E. Blankenship, D. M. Tiede, J. Barber, G. W. Brudvig, G. Fleming, M. Ghirardi, M. R. Gunner, W. Junge, D. M. Kramer, A. Melis, T. A. Moore, C. C. Moser, D. G. Nocera, A. J. Nozik, D. R. Ort, W. W. Parson, R. C. Prince and R. T. Sayre, *Science*, 2011, **332**, 805–809.
145 S. Hoyer, A. Ishizaki and K. B. Whaley, 2011, arXiv:1106.2911v1.
146 F. Galve, L. A. Pachón and D. Zueco, *Phys. Rev. Lett.*, 2010, **105**, 180501.
147 V. Vedral, *Nature*, 2010, **468**, 769–770.
148 M. A. Martín-Delgado, J. Rodriguez-Laguna and G. Sierra, *Phys. Rev. B*, 2002, **65**, 155116.
149 J. Prior, A. W. Chin, S. F. Huelga and M. B. Plenio, *Phys. Rev. Lett.*, 2010, **105**, 050404.
150 A. W. Chin, J. Prior, R. Rosenbach, F. Caycedo-Soler, S. F. Huelga and M. B. Plenio, *Vibrational structures and long-lasting electronic coherence*, 2012, arXiv:1203.0776v1.